

Hybrid Metamaterial Optical Tweezers for Dielectric Particles and Biomolecules Discrimination

Domna G. Kotsifaki,^{*,†,‡} Viet Giang Truong,[‡] Mirco Dindo,[¶] Paola Laurino,^{¶,§}
and Síle Nic Chormaic^{*,‡}

[†]*Photonics Lab, Division of Natural and Applied Sciences, Duke Kunshan University, 8
Duke Ave, Kunshan, Jiangsu Province 215316, China*

[‡]*Light-Matter Interactions for Quantum Technologies Unit, Okinawa Institute of Science
and Technology Graduate University, Onna, Okinawa 904-0495, Japan*

[¶]*Protein Engineering and Evolution Unit, Okinawa Institute of Science and Technology
Graduate University, Onna, Okinawa 904-0495, Japan*

[§]*Institute for Protein Research, Osaka University, Suita, Osaka 565-0871, Japan*

E-mail: dk310@duke.edu; sile.nicchormaic@oist.jp

Abstract

Although plasmonic nanotweezers can achieve manipulation on a scale smaller than the diffraction limit, direct trapping of sub-10 nm bioparticles in an aqueous environment without modifications remains challenging. Here, we demonstrate enzyme delivery-trapping and dynamic manipulation at the single-entity level by employing photothermal-assisted trapping via metamaterial optical tweezers at low trapping laser intensities. By analyzing the probability density function, we are able to distinguish dielectric particles from biomolecules. For enzyme-related data, the presence of two

peaks in violin plots indicates conformational changes or interactions with the environment. We also observe that increasing the laser intensity increases the local temperature, resulting in enzyme aggregation. This study provides an alternative approach for identifying single enzymes and dielectric particles by combining plasmonic fields and photothermal heat, while paving the way for label-free characterization of biomolecules at the single-particle level.

Keywords: Metamaterial optical tweezers, enzyme trapping, thermoplasmonics, single-particle level, violin plots, aggregations

Introduction

In biomedical research and disease diagnosis, detecting single biomolecules in solution is essential. It allows for a better understanding of disease mechanisms, leading to early detection, and treatment responses. Several advanced techniques and methods are used to meet this goal.¹ For example, fluorescence resonance energy transfer (FRET) can be used to detect conformational changes by measuring the transfer of energy between two fluorophores attached to interacting biomolecules.² However, repeated excitation of fluorophores can lead to photobleaching, reducing the intensity of fluorescence signals over time which may affect the accuracy of measurements.³ Since optical tweezers⁴ can measure forces and torques with high accuracy and temporal resolution, they could be considered as a preferred method for single-particle detection in many biophysical applications.⁵ Optical tweezers have been employed to investigate the movement of motor proteins such as kinesin⁶ and myosin,⁷ as well as to measure the elasticity, stretching, and torsional properties of DNA^{5,8,9} and RNA.^{5,8} Despite the wide range of applications,^{10,11} optical tweezers face certain challenges, particularly when it comes to tethering and labelling molecules. To overcome the limitations of conventional optical tweezers for detecting single molecules, plasmonic optical tweezers (POT) were developed.^{12–16} With the ability of metallic nanostructures to concentrate light

in subwavelength volumes, POT techniques allow precise manipulation of nanoscale objects, such as biomolecules,^{15,17,18} nanoparticles,^{19–21} and quantum dots.^{22,23} For example, double nanohole optical tweezers were used to investigate how protein p53 interacts with a single DNA-hairpin,¹⁸ to measure vibrational modes of proteins in the low-wavenumber regime,²⁴ and to monitor the structure dynamics of single enzymes during catalytic cycles.²⁵

Among all nanostructure designs, metamaterials have emerged as the most promising owing to their exotic electromagnetic properties and functionalities that are not attainable from naturally occurring materials.²⁶ In biosensing, metamaterials provide the large active area necessary for the assessment and quantification of interactions between the resonating metamolecules and biological entity.^{27–31} Exploiting this advantage, several metamaterials have been designed to detect viruses,²⁸ bacteria³¹ and other biomolecules.²⁹ Metamaterials that support a Fano-like resonance are characterized by a narrow spectral window where scattering is suppressed and absorption is enhanced due to interference between super-radiant and subradiant plasmonic modes.³² The resonance of these nanostructures is extremely sensitive to their geometric characteristics and, in combination with subdiffraction volumes, can be employed for applications such as ultrasensitive protein recognition^{29,33} and efficient nanoparticle trapping using low trapping laser intensities.^{16,34,35}

Meanwhile, the energy losses of plasmonics and the associated heat generation at the nanoscale could benefit a broad range of applications, including photothermal-assisted plasmonic sensing.³⁶ Specifically, the localized heat generated by metallic nanostructures can lead to changes in the refractive index of the surrounding medium that are detectable and can be correlated with analyte concentrations.³⁷ For instance, dual-functional plasmonic biosensors have been demonstrated to facilitate the specific nucleic acid hybridization of SARS-CoV-2, while simultaneously detecting the nonamplified nucleic acid sequences of the virus.³⁷ This finding suggests that plasmonics and near-field heating also have the potential to regulate the biocatalytic behaviors of the site-specific nucleases, leading to accurate biomolecule detection and discrimination.³⁷

In this work, we extend the utility of metamaterial optical tweezers and introduce a thermoplasmonic-assisted concept to optically trap and discriminate between dielectric nanoparticles and biomolecules in the nanoscale regime. We used 20 nm diameter polystyrene beads and urease that has a hydrodynamic radius of 7 nm suspended in polyethylene glycol(PEG)/heavy water solution. Urease is a nickel-containing enzyme that catalyzes the hydrolysis of urea to form ammonia and carbon dioxide in some bacteria, fungi, algae, and plants.^{38,39} Healthy human organisms do not contain urease; however, *Helicobacter pylori*, a bacterial pathogen of the human stomach and a class I carcinogen,^{40,41} secretes urease.⁴² PEG is a highly soluble polymer in water that has been used to modify biomolecules and to create more stable drug delivery systems for anticancer therapies.⁴³ We observed that a single urease can be delivered to, and trapped in, the nano-aperture of the asymmetric, split-ring (ASR) metamaterial for trapping laser intensities lower than $0.5 \text{ mW}/\mu\text{m}^2$. Due to the large hydrodynamic motion and conformational changes of the molecule in the plasmonic hotspot, two peaks appeared in the probability density function for single and multiple trapping events of ureases. For dielectric particles, violin plots show a single peak both for single and multiple trapping events, indicating their consistent behavior during the trapping process. Furthermore, we investigated how the normalized root-mean-square of the first urease trapping event changes with trapping laser intensities and trap stiffness and we conclude that aggregations of molecules may form and be trapped for intensities greater than $1 \text{ mW}/\mu\text{m}^2$, *i.e.*, at high temperatures. We also measured the average time until the first observed trapping event occurred for several molecular concentrations. Using the same range of trapping laser intensities, average trapping times for low molecule concentrations were measured as being similar to those for non-bioparticle trapping. According to our analysis, our metamaterial optical tweezer platform facilitates the identification of various particles in a simple and label-free way and this may open up new avenues for nanoscience and life science research.

Materials and Methods

A schematic of the experimental setup used to trap and manipulate a single enzyme molecule is shown in Figure 1. The optical tweezers consist of a 930 nm continuous-wave (CW) laser focused using a high numerical aperture ($NA = 1.3$) oil immersion objective lens (OLYMPUS UPlanFL N 100 \times) to a spot size of 1 μm . Detection of trapping events was conducted by collecting the transmitted laser light through a 50 \times objective lens (Nikon CF Plan), sending it to an avalanche photodiode (APD430A/M, Thorlabs), and recording it using a data acquisition card (DAQ) at a frequency of 100 kHz with LabVIEW software.

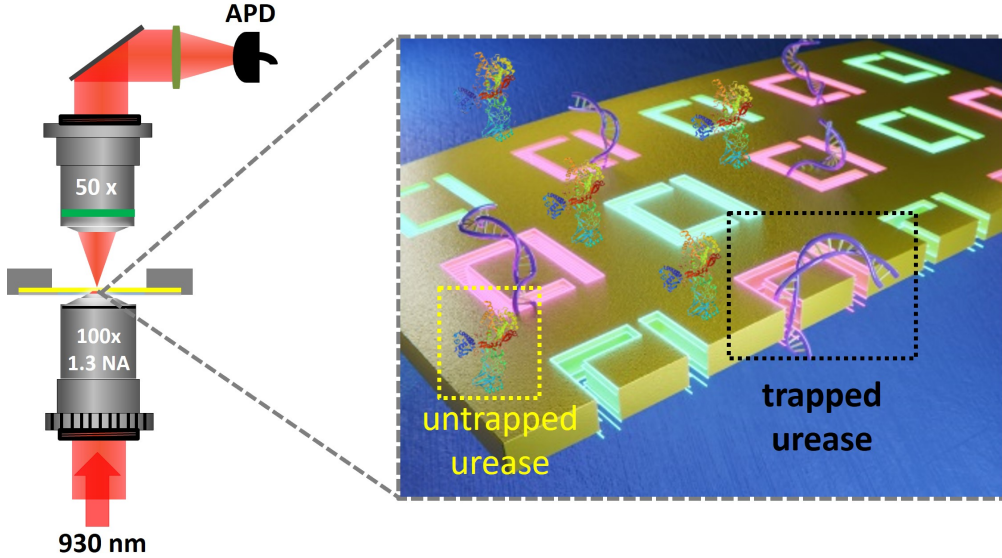


Figure 1: Schematic of the plasmonic optical tweezers setup used to demonstrate single biomolecule trapping. The incident laser beam from the high numerical aperture objective lens (100 \times -1.3 NA) is collected by the upper objective lens (50 \times) and detected with an avalanche photodiode (APD). An artistic representation of the optically trapped enzyme in the excited plasmonic hotspot is shown. The urease is made up of a single-chain polypeptide containing 840 amino acid residues.⁴⁴ Because urease's conformation may change when trapped, the trapped enzyme has been drawn in modified structures within the nano-aperture compared with its structure in a free solution.

The unit cell of the metamaterial contains an asymmetrically split ring (ASR) consisting of two nano-apertures in a gold film (Figure 2(a)). The full array consists of 15 (x -direction) \times 16 (y -direction) units with a period of 400 nm and was fabricated using focused ion beam

(FIB-FEI Helios G3UC) milling on a 50 nm thin gold film (PHASIS, Geneva, BioNano) at 30 kV and a 2 pA beam current. The metamaterial was attached to a microscope cover glass with adhesive microscope spacers of 10 μm thickness, forming a microwell. Since the focus spot has a diameter of about $\sim 1 \mu\text{m}$ means that 2×2 metamolecules of the metamaterial structures were illuminated. We used a solution containing heavy water, polyethylene glycol (PEG₆₀₀₀), and urease (U4002; Sigma-Aldrich). Several concentrations of urease suspended in the 0.4 %w/v PEG₆₀₀₀/D₂O water solution were used and a microwell containing urease of various concentrations was mounted and fixed on top of a piezoelectric translation stage. The urease protein could then be trapped by plasmon-enhanced optical forces into the ASR nano-aperture of the metamaterial. In addition, a solution of polystyrene (PS) particles with a mean diameter of 20 nm (ThermoFisher Scientific, F8786) in 0.4 %w/v PEG₆₀₀₀/D₂O water with a concentration of 0.0625% w/v was used as a control.

Results and Discussion

We performed finite-difference time-domain simulations using COMSOL Multiphysics software to calculate the electric field enhancement of the metamaterial (Figure 2(b)). The incident light was polarized along the y -axis. The mesh had a minimum size of 1.2 nm, maximum size of 44 nm, and resolution of narrow regions, *i.e.* the region of the titanium adhesion layer, at 0.7 nm. Using the shape of the metamaterial as determined by a scanning electron microscopy image (SEM), we determined the resonance wavelength in the absorption spectrum to be at 932 nm, just slightly above the 930 nm wavelength of the trapping laser.³⁴ Enhanced light absorption results in a temperature increase and thermal gradient in the fluid. Figure 2(c) shows the increase in temperature due to laser irradiation of $1 \text{ mW}/\mu\text{m}^2$ on the metamaterial. We note that, at the center of the metamaterial, the strong heat source density leads to the temperature increase being around 10 K, while far from the center the heat source is weaker and the temperature of the structure does not change appreciably.

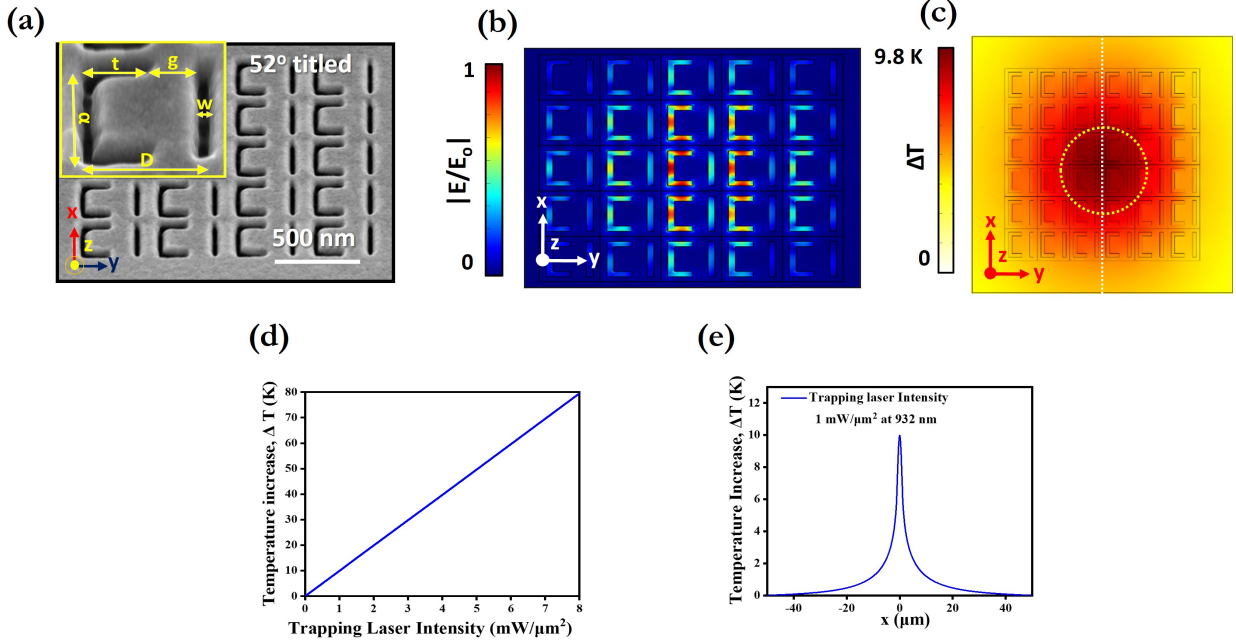


Figure 2: (a) Scanning electron microscopy (SEM) image of a 6×6 array of the asymmetric split-ring (ASR) metamaterial fabricated from a 50 nm thin gold film, taken at an angle of 52° to the surface normal. The inset shows a metamolecule unit with feature dimensions: $D = 400 \pm 2$ nm, vertical slit $\alpha = 310 \pm 3$ nm, horizontal slit $t = 165 \pm 3$ nm, gap $g = 100 \pm 3$ nm, and slit width $w = 44 \pm 2$ nm. (b) Simulated spatial distribution of the electric field enhancement of the metamaterial in the xy -plane at a wavelength of 930 nm. (c) Simulated temperature increase distribution for $1 \text{ mW}/\mu\text{m}^2$ illumination at 930 nm from the bottom of the metamaterial (from the glass layer) in the xy -plane. The yellow dotted line shows the laser beam spot size. (d) Numerical simulation of the average temperature increase as a function of the trapping laser intensity. (e) Numerical simulation of the evolution of the temperature increase with the distance from the center of the metamaterial for $1 \text{ mW}/\mu\text{m}^2$ illumination (for the white dotted line in Fig. 2(c)).

The simulated temperature change versus trapping laser intensity (I_{trap}) is shown in Figure 2(d). Because the gold has high thermal conductivity compared with the surrounding medium, as expected from the heat diffusion equation,⁴⁵ the temperature distribution in the metamaterial remains fairly uniform and increases linearly as a function of I_{trap} . Notably, at $8.0 \text{ mW}/\mu\text{m}^2$ the temperature increase in the metamaterial is predicted to exceed 80 K. This is not a negligible value and shows that the metamaterial is unable to dissipate heat from a focused laser beam at high trapping laser intensities. In addition, Figure 2(e) shows how the temperature increase changes as a function of distance from the center of the metamaterial.

We observe that the temperature increase is reduced by 50% at $1.5\ \mu\text{m}$ from the center for a laser intensity of $1\ \text{mW}/\mu\text{m}^2$. Therefore, our metamaterial structure has the ability to deliver and trap sub-10 nm particles such as small protein molecules without the risk of photo-induced damage.

Since the resonance frequency of a metamaterial is sensitive to small changes in the local refractive index, the presence of biomolecules in the ASR nano-aperture can be tracked by changes in the transmitted signal. Figure 3(a) shows the time evolution of the transmitted signal as measured on the APD through the ASR metamolecules in the presence of urease solution. The abrupt jump in the APD signal at about 21 s and the change in the noise level right after the jump are signatures of biomolecular trapping by the metamaterial. In a control experiment, using a solution without urease molecules, no changes in the transmission signal were observed, confirming that the jump can be attributed to the trapping of urease molecules. Additionally, the cycle of trapping and then releasing the enzyme was repeated by blocking and unblocking the trapping laser beam.

Two specific properties were extracted from the signal of each trapping event, the root-mean-square (RMS or σ) deviation of the transmitted laser signal as measured on the APD, and the trap stiffness, k . The RMS of the transmitted signal was calculated by fitting a Gaussian distribution to its histogram. Figures 3(b) and (c) show the transmitted signal fluctuations with corresponding histograms for the two different states, *i.e.*, vacant and trapped. The width of the Gaussian distribution for the vacant case displays a small RMS deviation, *i.e.*, $\sigma = 0.0031\ \text{V}$, while the RMS for the trapped event, $\sigma = 0.0166\ \text{V}$, is significantly larger. For comparison, we show a sequence of trapping and releasing events of a 20 nm PS particle in an array of ASRs in Figure 3(d). As we illuminated 2×2 metamolecules, we excited eight plasmonic hotspots, which can trap up to eight nanoparticles.³⁴ Therefore, we assume that each jump in the APD signal corresponded to a single trapping event. Figures 3(e) and (f) show fluctuations in the APD signal with corresponding histograms as well as the Gaussian fit for the trapped nanoparticle and the vacant positions. Similarly to the case for urease,

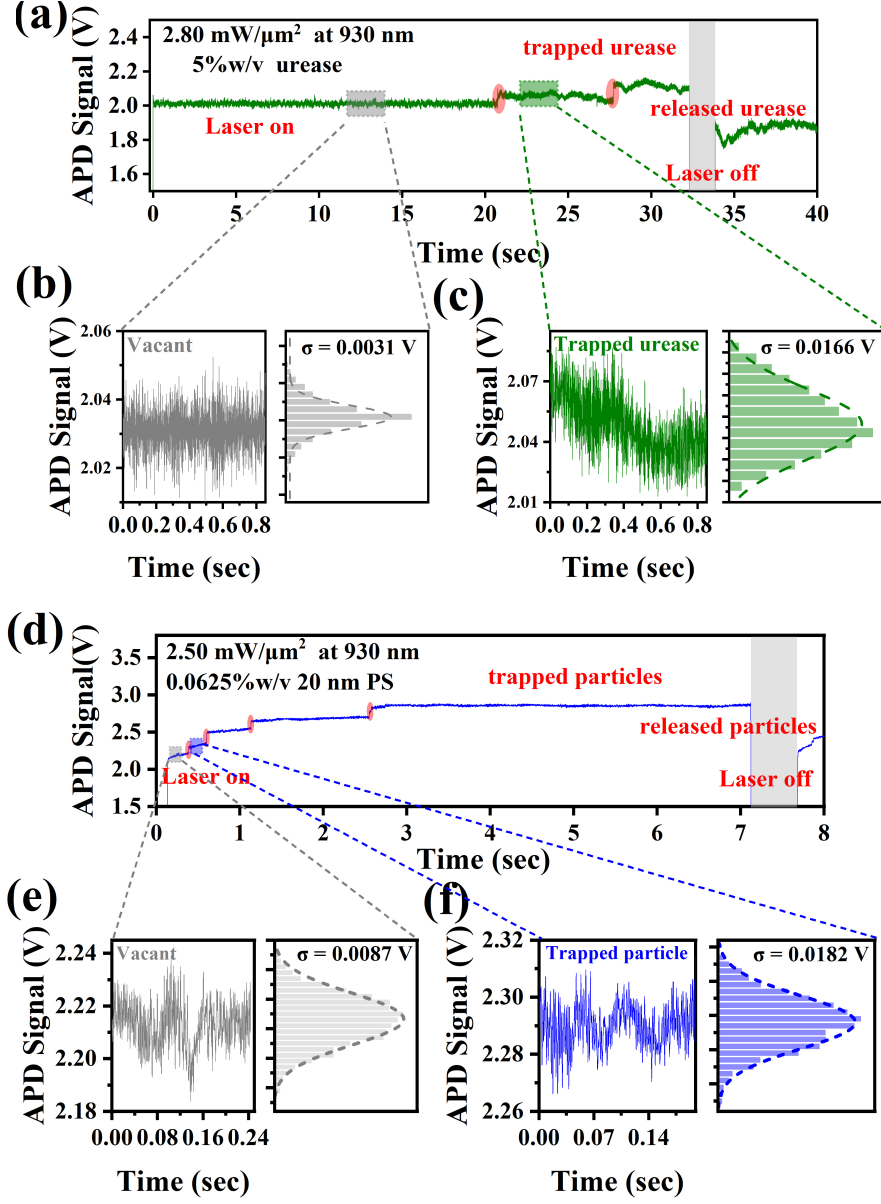


Figure 3: (a) Time trace of optical transmission through the ASR metamaterial, showing the optical trapping of a single urease molecule as a sudden discrete jump in the APD signal at 21 s. A few seconds later another jump indicates a second trapping event. A trapping laser wavelength of 930 nm and laser intensity at the sample plane of $2.80 \text{ mW}/\mu\text{m}^2$ were used. Transmission signal fluctuations and the Gaussian fit (dashed lines) to the corresponding histogram of the transmitted signal fluctuations in case of (b) vacant (grey box in (a)) and (c) trapped (green box in (a)) states of the urease protein. (d) Time trace of optical transmission through the ASR metamaterial, showing the optical trapping of a 20 nm polystyrene particle. A trapping laser intensity at the sample plane of $2.50 \text{ mW}/\mu\text{m}^2$ was used. Transmission signal fluctuations and the Gaussian fit (dashed lines) to the corresponding histogram of the (e) vacant (grey box in (d)) and (f) trapped (blue box in (d)) states of the PS nanoparticle. The width of the Gaussian distribution, σ , shows the root-mean-square variation of the transmitted signal.

we observe that the APD signal for trapped PS nanoparticles has a larger RMS deviation than that observed for no trapping event. Comparing Figure 3(c) with Figure 3(f), we notice that, in the case of protein trapping, the signal fluctuations are larger than for PS particle trapping. We assume that the hydrodynamical motion and conformational changes of the protein in the ASR may increase fluctuations in the transmitted intensity of the trapping laser.^{46,47} The intensity of the transmitted signal at the trapping site (I) is proportional to the trapping potential energy (U) which itself is proportional to the polarizability²⁴ of the trapped particle; hence, the RMS deviation of the trapping laser signal may scale with the polarizability of the trapped biomolecule (*i.e.* the potential energy of a Rayleigh particle can be written in the dipole limit as $U = (\alpha |E|^2)/2$ where α is the polarizability of the particle and E is the electric field).⁴⁶ Moreover, the biomolecule's polarizability is proportional to its volume, V , and the volume scales with the mass. Since RMS (σ) scales with the polarizability and the polarizability scales with the mass, we conclude that the $\sigma \propto M$. Therefore, by calculating the RMS deviation of the transmitted signal for each trapping event, the total molecular weight of the trapped enzyme at the plasmonic hotspots of the metamaterial can be estimated.

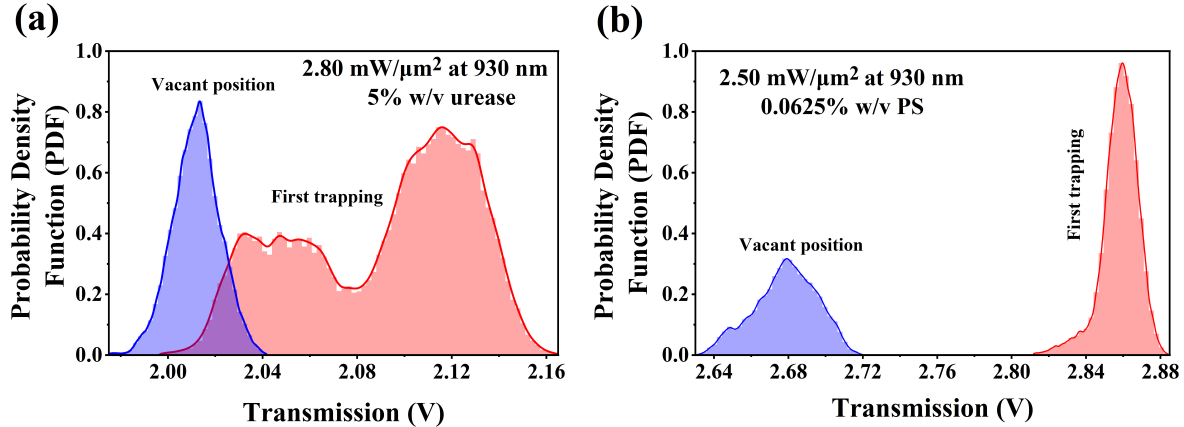


Figure 4: Probability density function (PDF) of the APD signal calculated from 10 s traces before (purple curve) and after trapping (red curve) for (a) 7 nm urease molecules, and (b) 20 nm polystyrene particles. The solid line in all graphs is the fitting of the kernel density distribution.

In addition, we calculated the probability density function (PDF) of the APD signal through the metamaterial both before (purple curve) and after (red curve) trapping of urease and polystyrene nanoparticles (Figures 4(a) and (b)). In this case, the PDF refers to the likelihood of finding the trapped particle in a specific arrangement or exhibiting a particular characteristic.⁴⁸ We observe that trapping urease leads to a PDF with a wider amplitude distribution with two peaks compared to the vacant signal. This might indicate heterogeneity in enzyme activity, conformational states, or interactions with the environment.²⁵ However, the PDF calculated from the PS nanoparticle trapping signal shows a relatively narrow peak compared to the vacant signal (Figure 4(b)). This observation reveals that the PS nanoparticles behave more uniformly or consistently when trapped. Urease and PS nanoparticles have different sizes, shapes, and optical properties. These characteristics can influence their trapping behavior and result in different PDF shapes. Therefore, the width and the shape of the PDF may be a key factor to distinguish the behavior of the particles in optical trapping applications.

To further investigate the behavior of enzymes when trapped, we calculated the PDFs of the changes in the APD signal through the metamaterial for multiple trapping events for both types of particles. For this purpose, we defined and calculated the relative transmitted APD signal as $(T_i - T_{i-1})/T_i$, where T_i is the transmitted signal for each trapping event, T_{i-1} is the transmitted signal one trapping step/jump before and i is the number of trapping events ($i = 1, 2, 3, 4 \dots$ trapping steps). This method minimizes effects caused by previously trapped particles, the metamaterial structure, and instrumentation noise. Note that by changing the trapping laser power and the trapping duration, we observed single or multiple trapping events. In Figure 5(a), we present violin plots for both types of particles at the lowest laser intensity for which we observed trapping. Violin plots are a data visualization tool that combines aspects of box plots and kernel density plots to represent the distribution of the experimental data.⁴⁸ Using this method when studying enzymes, for example, can reveal the heterogeneity of enzyme properties or conformational states under several experimental

conditions.⁴⁸ Additionally, monitoring the median in a violin plot helps us to understand how the average behavior of the trapped particle is affected by various trapping conditions.⁴⁸ In our case, the data set for the urease molecules has a median (white dot in Figure 5(a)) of the same magnitude as the data set obtained for PS nanoparticle trapping as a result of the normalization of the data. By comparing medians for nanoparticle and enzyme trapping experimental data, we can confirm that any effects due to the laser intensity differences are minimized. We also note that the violin plot for urease shows two peaks, while that for polystyrene displays only one.

Next, we generated violin plots for multiple trapping events for both polystyrene and urease particles. Note that we did not observe multiple urease trapping events for every laser trapping power used to illuminate the metamaterial, whereas we did for the PS particles. Hence, here we analyze data where up to four trapping events were observed for both types of particles at similar I_{trap} . In Figure 5(b) we present the violin plots of four PS nanoparticle trapping events. Due to polystyrene’s homogeneous nature, all violin plots show a peak, hence the data may have similar characteristics. Furthermore, we observe that the elongated kernel density distribution slightly decreases with increasing trap steps from one to four. The decrease in elongation of the PDF may suggest that the trapping strength increases as the number of trapping events increases. In the case of enzyme trapping at low (Figure 5(a)) and high (Figure 5(c)) trapping laser intensities, whether for a single trapping event or multiple events, two peaks appear in the violin plots with a roughly constant elongated distribution in contrast to the PS nanoparticle trapping. Proteins, such as enzymes, are held together by various weak interactions, including hydrogen bonds, van der Waals forces, and hydrophobic interactions. Hence, as the temperature rises, the thermal energy can overcome these weak interactions, leading to changes in protein conformation. Since urease is sensitive to changes in temperature,⁴⁹ its structural conformation can be modulated by the local temperature increase on the metamaterial. Hence, we conclude that the presence of these two peaks for the enzyme-related data suggests conformational changes in the protein.^{48,50}

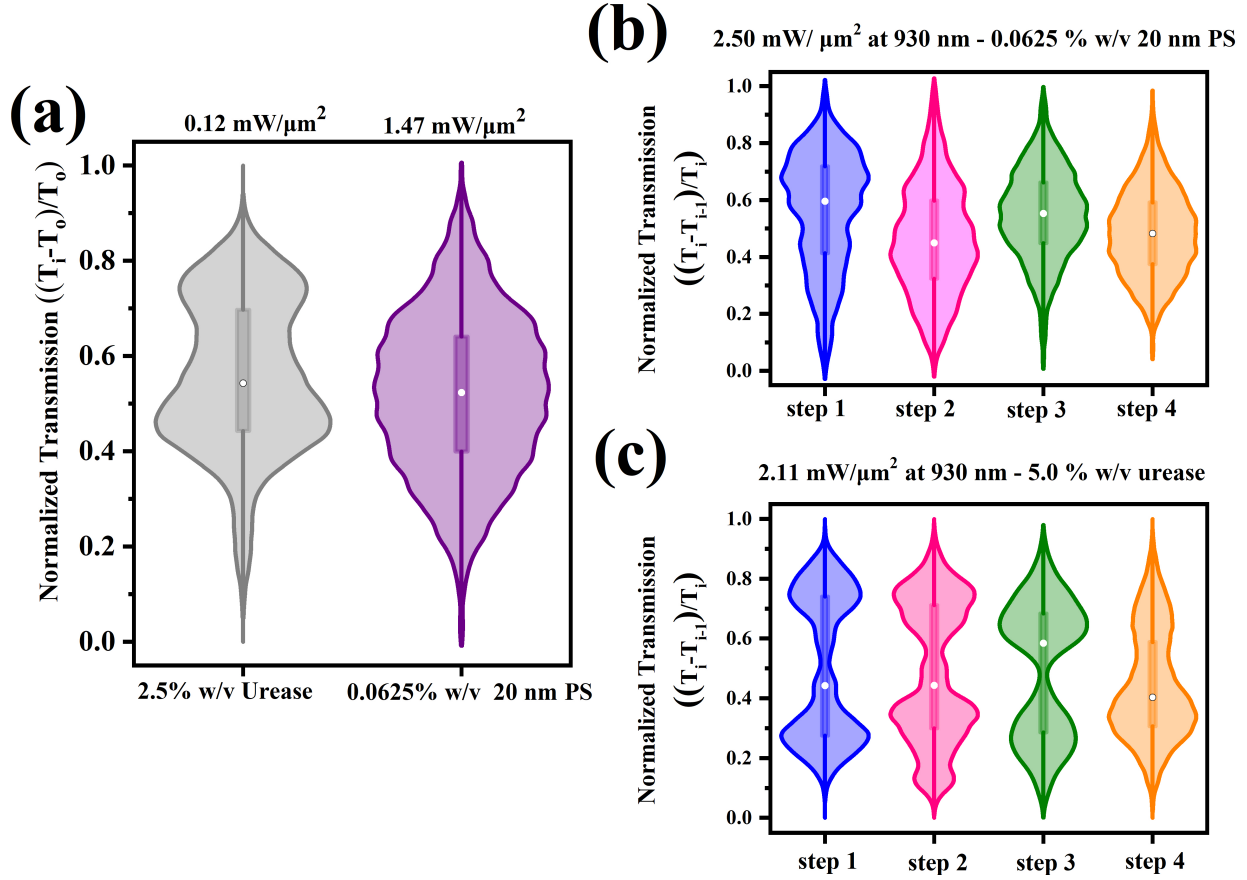


Figure 5: (a) Violin plots for the first trapping event for a urease molecule with a concentration of 2.5% w/v (grey plot) and for a 20 nm polystyrene particle with a concentration of 0.0625% w/v (purple plot). For urease trapping, the I_{trap} was 0.12 $\text{mW}/\mu\text{m}^2$ while for PS particles it was 1.4 $\text{mW}/\mu\text{m}^2$. (b) Violin plots for multiple trapping events of 20 nm PS particles at a I_{trap} of 2.50 $\text{mW}/\mu\text{m}^2$ and a concentration of 0.0625% w/v. (c) Violin plots for multiple trapping events of urease molecules at a I_{trap} of 2.11 $\text{mW}/\mu\text{m}^2$ and a concentration of 5.0% w/v. The wavelength of the trapping laser was 930 nm.

We subsequently calculated the normalized root-mean-squared, *i.e.* NRMS, of the transmitted signal recorded on the APD for the first trapping event as a function of the incident I_{trap} for different urease concentrations and a PS nanoparticle concentration of 0.0625% w/v using a 5 s measuring window (Figure 6(a)). We notice that, for I_{trap} less than 1 mW/ μm^2 , the NRMS values of the APD signal for urease are roughly constant for all concentrations. As the I_{trap} increases, the NRMS of the APD signal increases, revealing an exponential-type behavior. By increasing the trapping laser intensity, more energy is transferred to the trapped molecule, resulting in greater hydrodynamic movement and large conformational fluctuations of the molecule in the harmonic trap, leading to an increase in the NRMS of the transmitted signals.⁴⁷ On the other hand, we notice a constant NRMS of the APD signal for PS trapping as a function of trapping laser intensity. This arises due to the difference in properties between urease and polystyrene, *i.e.* the enzyme is not perfectly spherical and solid.

Additionally, we also calculated the trap stiffness ($\kappa = \gamma/\tau$) of the enzyme and the PS nanoparticle using the transient time method.⁵¹ For urease, we assumed a distance of 17 nm between the trapped molecule and ASR metamolecule wall¹⁶ to modify the Faxén correction, γ . We used the viscosity of water at room temperature⁵² and a hydrodynamic radius of 7 nm for urease.³⁹ We noted a linear dependence of trap stiffness versus laser intensity (data not shown here). In Figure 6(b), we plot the NRMS of the APD transmitted signal as a function of trap stiffness and urease concentrations. The NRMS of the APD signal provides information on the fluctuation of the trapped particle inside the ASR metamolecule while the trap stiffness shows the strength of the optical forces exerted on the trapped particle. We observe that the NRMS of the recorded signal calculated for a 20 nm PS particle remains constant as the trap stiffness increases, *i.e.*, as I_{trap} increases (Figures 6(a) and (b)). Note that the trap stiffness scales with the radius cubed, *i.e.*, the volume (assuming a spherical particle), leading to a scaling with the mass of the particle assuming uniform density, (*i.e.*, $k \propto M$). As a result of the constant NRMS values for PS particles versus trap

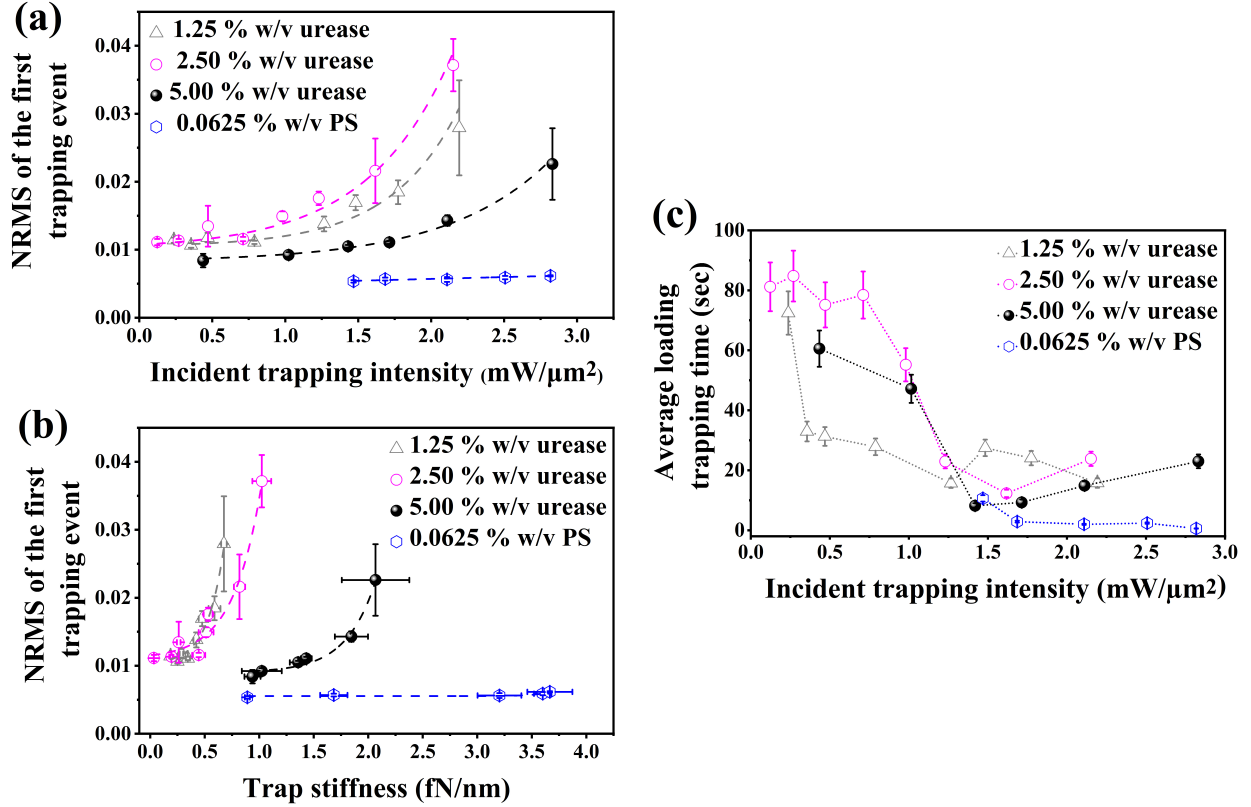


Figure 6: (a) Normalized root-mean-squared, NRMS, of the transmitted signal on the APD for the first trapping event as a function of I_{trap} and urease concentrations. The dashed lines are the exponential fits to the experimental data. The plot for a 20 nm PS particle is also included (blue). (b) NRMS of the transmitted signal on the APD for the first trapping event as a function of the trap stiffness and urease concentrations. The dashed lines are the exponential fits to the experimental results. The plot for a 20 nm PS particle is included (blue). (c) Average urease trapping time as a function of I_{trap} and concentrations. The average PS particle trapping time is included (blue). The error bars for each figure are the standard deviation of the experimental data which has been calculated by three data sets for each point.

stiffness, we conclude that a single PS particle is trapped in the ASR during each experiment. For the low urease concentrations (magenta and grey lines in Figure 6(b)), and incident I_{trap} less than $0.5 \text{ mW}/\mu\text{m}^2$, we also observe the NRMS value of the transmitted signal for urease to be constant with trap stiffness when the concentration is low. We assume in this regime that single urease trapping was achieved. In addition to trap stiffness increasing as trapping laser intensity increases, the local temperature within the microwell also increases. With

an increase in temperature, urease undergoes denaturation, where the three-dimensional structure is disrupted, causing aggregation.^{49,53} Moreover, it has been reported that urease becomes thermally inactive at 80°C.⁵³ Consequently, enzyme aggregates may form as the trapping laser intensities increase, leading to an increase in the molecular weight and its hydrodynamic radius, resulting in trap stiffness increases. In other words, we assume that for I_{trap} above 1 mW/ μm^2 , aggregations of urease were trapped. Note that the melting point of urease is around 140°C,⁵⁴ which can be achieved at I_{trap} beyond 8.0 mW/ μm^2 based on Figure 2(d), therefore we did not exceed this value in any of our experiments.

Finally, we investigated the average time taken to trap urease molecules as a function of the trapping laser intensity for different molecular concentrations (Figure 6(c)). The trapping time is defined as the time from when the trapping laser is turned on ($t_o = 0$) to the transmission signal's first observed discrete step, indicating the first trapping event. We calculated the experimental trapping time based on the average values of two runs. As noted in our previous works,^{55,56} we assumed that convection fluid flow occurs as the I_{trap} increases, which causes the temperature increase. As a result, the probability of trapping a urease molecule in the fluid flow increases, thence delivering it to the illuminated area of the metamaterial, thus reducing the average trapping time. Specifically, the average time until the first trapping event observed was calculated to be 16 s, 23 s, 47 sec, and 11 s for concentrations of 1.25% w/v and 2.50%w/v for urease, and 5.00% w/v for PS particles, respectively, at a I_{trap} of around 1 mW/ μm^2 . When the enzyme concentration increases, we observed that the trapping time increased slightly as there are more molecules available to move and spread out. In other words, as more molecules are present in a given space, they may experience increased collisions and interactions with neighboring molecules. This crowding effect may delay the trapping process and result in a slight increase in the trapping time compared to that observed for a low urease concentration. However, this change in enzyme concentration did not strongly alter the rapid delivery of the molecule to the metamaterial surface but rather modified the absolute values of the enzyme trapping

times. We also note that PS nanoparticle trapping required similar diffusion times as urease molecules at the lowest concentrations.

Conclusions

Through the manipulation of light and mass transfer at a liquid/metamaterial interface, we have demonstrated a versatile nanofluidic system on a chip that enables nano-object transportation, trapping, and identification. Using low trapping laser intensities, we successfully delivered and trapped single biomolecules using a metamaterial. We showed that the optical trapping signals from the same metamaterial but for different types of particles provide two parameters that allow us to discriminate their properties. By calculating the probability density function, we succeeded in distinguishing a dielectric from a biomolecule particle. Specifically, we used violin plots to study the differences; a single peak was observed for PS nanoparticle trapping, characteristic of a homogeneous particle, while two peaks appeared in the case of urease trapping due to the anisotropic nature of the molecule. The second parameter considered was a combination of the normalized-root-mean-square of the transmitted signal and the trap stiffness that confirmed the aggregation of the biomolecule and trapping of aggregates at I_{trap} larger than $1 \text{ mW}/\mu\text{m}^2$. Understanding the factors that contribute to protein aggregation and developing strategies to prevent or control it are critical for both biomedical research and in the pharmaceutical industry. This will be a subject of our future work. In summary, our noninvasive optical nanotweezers approach is expected to open new avenues in nanoscience and life science research by offering an unprecedented level of control of and discrimination between nano-objects without the limitations of strong bonding fluorescent groups, thereby making single biomolecule manipulation and characterization a reality.

Acknowledgement

The authors thank M. Ozer for technical assistance, N. Ishizu from the Engineering Section at Okinawa Institute of Science and Technology Graduate University (OIST), P. Puchikov from the Scientific Computing and Data Analysis Section at OIST, T. Bouloumis for the device fabrication. SNC acknowledges initial discussions with F.A. Samatey and M.A. Price on protein structure and detection methods. This work was supported by funding from OIST Graduate University. DGK acknowledges support from the JSPS Grant-in-Aid for Scientific Research (C) Grant Number GD1675001 and the Sumitomo Foundation Grant for Basic Science Research Project.

References

- (1) Farka, Z.; Mickert, M. J.; Pastucha, M.; Mikušová, Z.; Skládal, P.; Gorris, H. H. Advances in Optical Single-Molecule Detection: En-Route to Supersensitive Bioaffinity Assays. *Angewandte Chemie International Edition* **2020**, *59*, 10746–10773.
- (2) Rahul, R.; Sungchul, H.; Taekjip, H. A practical guide to single-molecule FRET. *Nature Methods* **2008**, *5*, 507–516.
- (3) Leavesley, S. J.; Rich, T. C. Overcoming limitations of FRET measurements. *Cytometry Part A* **2016**, *89*, 325–327.
- (4) Ashkin, A. Acceleration and Trapping of Particles by Radiation Pressure. *Phys. Rev. Lett.* **1970**, *24*, 156–159.
- (5) Bustamante, C. J.; Chemla, Y. R.; Liu, S.; Wang, M. D. Optical tweezers in single-molecule biophysics. *Nature Reviews Methods Primers* **2021**, *1:25*, 1–25.
- (6) Svoboda, K.; Schmidt, C. F.; Schnapp, B. J.; Block, S. M. Direct observation of kinesin stepping by optical trapping interferometry. *Nature* **1993**, *365*, 721–727.

- (7) Cappello, G.; Pierobon, P.; Symonds, C.; Busoni, L.; Christof, J.; Gebhardt, M.; Rief, M.; Prost, J. Myosin V stepping mechanism. *Proceedings of the National Academy of Sciences* **2007**, *104*, 15328–15333.
- (8) Zev, B.; Michael D., S.; Jeff, G.; B., S.; Smith, N. R.; Cozzarelli, C.; Bustamante Structural transitions and elasticity from torque measurements on DNA. *Nature* **2003**, *424*, 338–341.
- (9) Allemand, J.-F.; Bensimon, D.; Croquette, V. Stretching DNA and RNA to probe their interactions with proteins. *Current Opinion in Structural Biology* **2003**, *13*, 266–274.
- (10) Yang, Y.; Ren, Y.; Chen, M.; Arita, Y.; Rosales-Guzmán, C. Optical trapping with structured light: a review. *Advanced Photonics* **2021**, *3*, 034001.
- (11) Zhu, Z.; Zhang, Y.; Zhang, S.; Adam, A. J. L.; Min, C.; Urbach, H. P.; Yuan, X. Nonlinear optical trapping effect with reverse saturable absorption. *Advanced Photonics* **2023**, *5*, 046006.
- (12) Novotny, L.; Bian, R. X.; Xie, X. S. Theory of Nanometric Optical Tweezers. *Phys. Rev. Lett.* **1997**, *79*, 645–648.
- (13) Crozier, K. B. Plasmonic Nanotweezers: What’s Next? *ACS Photonics* **0**, *0*, null.
- (14) Reece, P. J.; Garcés-Chávez, V.; Dholakia, K. Near-field optical micromanipulation with cavity enhanced evanescent waves. *Applied Physics Letters* **2006**, *88*, 221116.
- (15) Gordon, R. Biosensing with nanoaperture optical tweezers. *Optics & Laser Technology* **2019**, *109*, 328–335.
- (16) Kotsifaki, D. G.; Truong, V. G.; Nic Chormaic, S. Fano-resonant, asymmetric, metamaterial-assisted tweezers for single nanoparticle trapping. *Nano Letters* **2020**, *20*, 3388–3395.

- (17) Pang, Y.; Gordon, R. Optical Trapping of a Single Protein. *Nano Letters* **2012**, *12*, 402–406.
- (18) Kotnala, A.; Gordon, R. Double nanohole optical tweezers visualize protein p53 suppressing unzipping of single DNA-hairpins. *Biomed. Opt. Express* **2014**, *5*, 1886–1894.
- (19) Wang, K.; Schonbrun, E.; Steinvurzel, P.; Crozier, K. B. Trapping and rotating nanoparticles using a plasmonic nano-tweezer with an integrated heat sink. *Nature Communications* **2011**, *2*, 469.
- (20) Wang, K.; Crozier, K. B. Plasmonic Trapping with a Gold Nanopillar. *ChemPhysChem* **2012**, *13*, 2639–2648.
- (21) Xu, Z.; Song, W.; Crozier, K. B. Direct Particle Tracking Observation and Brownian Dynamics Simulations of a Single Nanoparticle Optically Trapped by a Plasmonic Nanoaperture. *ACS Photonics* **2018**, *5*, 2850–2859.
- (22) Tsuboi, Y.; Shoji, T.; Kitamura, N.; Takase, M.; Murakoshi, K.; Mizumoto, Y.; Ishihara, H. Optical Trapping of Quantum Dots Based on Gap-Mode-Excitation of Localized Surface Plasmon. *The Journal of Physical Chemistry Letters* **2010**, *1*, 2327–2333.
- (23) Jiang, Q.; Roy, P.; Claude, J.-B.; Wenger, J. Single Photon Source from a Nanoantenna-Trapped Single Quantum Dot. *Nano Letters* **2021**, *21*, 7030–7036.
- (24) Wheaton, S.; Gelfand, R. M.; Gordon, R. Probing the Raman-active acoustic vibrations of nanoparticles with extraordinary spectral resolution. *Nature Photonics* **2015**, *9*, 68–72.
- (25) Ying, C.; Karakaci, E.; Bermudez-Urena, E.; Ianiro, A.; Foster, C.; Awasthi, S.; Guha, A.; Bryan, L.; List, J.; Balog, S.; Acuna, G. P.; Gordon, R.; Mayer, M. Watching single unmodified enzymes at work. 2021; <https://arxiv.org/abs/2107.06407>.

- (26) Luk'yanchuk, B.; Zheludev, N. I.; Maier, S. A.; Halas, N. J.; Nordlander, P.; Giessen, H.; Chong, T. C. The Fano resonance in plasmonic nanostructures and metamaterials. *Nature Materials* **2010**, *9*, 707–715.
- (27) Wang, Y.; Zhao, C.; Wang, J.; Luo, X.; Xie, L.; Zhan, S.; Kim, J.; Wang, X.; Liu, X.; Ying, Y. Wearable plasmonic-metasurface sensor for noninvasive and universal molecular fingerprint detection on biointerfaces. *Science Advances* **2021**, *7*, eabe4553.
- (28) Ahmadvand, A.; Gerislioglu, B.; Tomitaka, A.; Manickam, P.; Kaushik, A.; Bhansali, S.; Nair, M.; Pala, N. Extreme sensitive metasensor for targeted biomarkers identification using colloidal nanoparticles-integrated plasmonic unit cells. *Biomedical Optics Express* **2018**, *9*, 373–386.
- (29) Chihhui, W.; Khanikaev, A. B.; Adato, R.; Arju, N.; Ali, A. Y.; Altug, H.; Shvets, G. Fano-resonant asymmetric metamaterials for ultrasensitive spectroscopy and identification of molecular monolayers. *Nature Materials* **2012**, *11*, 69–75.
- (30) Wang, J.; Xu, Z.; Kotsifaki, D. G. Plasmonic and metamaterial biosensors: a game-changer for virus detection. *Sens. Diagn.* **2023**, *2*, 600–619.
- (31) Kotsifaki, D. G.; Singh, R. R.; Nic Chormaic, S.; Truong, V. G. Asymmetric splitting plasmonic nanostructures for the optical sensing of Escherichia coli. *Biomed. Opt. Express* **2023**, *14*, 4875–4887.
- (32) Papasimakis, N.; Zheludev, N. I. Metamaterial-induced transparency: sharp fano resonances and slow light. *Optics and Photonics News* **2009**, *20*, 22–27.
- (33) Ahmadvand, A.; Gerislioglu, B. Photonic and plasmonic metasensors. *Laser & Photonics Reviews* **2021**, *16*, 2100328.
- (34) Bouloumis, T. D.; Kotsifaki, D. G.; Nic Chormaic, S. Enabling self-induced back-action

- trapping of gold nanoparticles in metamaterial plasmonic tweezers. *Nano Letters* **2023**, *23*, 4723–4731.
- (35) Kotsifaki, D. G.; Truong, V. G.; Nic Chormaic, S. Dynamic multiple nanoparticle trapping using metamaterial plasmonic tweezers. *Applied Physics Letters* **2021**, *118*, 021107.
- (36) Guillaume, B.; Frank, C.; Romain, Q. Applications and challenges of thermoplasmonics. *Nature Materials* **2020**, *19*, 946–958.
- (37) Qiu, G.; Gai, Z.; Tao, Y.; Schmitt, J.; Kullak-Ublick, G. A.; Wang, J. Dual-Functional Plasmonic Photothermal Biosensors for Highly Accurate Severe Acute Respiratory Syndrome Coronavirus 2 Detection. *ACS Nano* **2020**, *14*, 5268–5277.
- (38) Blakeley, R. L.; Zerner, B. Jack bean urease: the first nickel enzyme. *Journal of Molecular Catalysis* **1984**, *23*, 263–292.
- (39) Follmer, C.; Pereira, F. V.; da Silveira, N. P.; Carlini, C. R. Jack bean urease (EC 3.5.1.5) aggregation monitored by dynamic and static light scattering. *Biophysical Chemistry* **2004**, *111*, 79–87.
- (40) Amieva, M. R.; El-Omar, E. M. Host-bacterial interactions in *Helicobacter pylori* infection. *Gastroenterology* **2008**, *134*, 306–323.
- (41) Lynch, D. A. F.; Mapstone, N. P.; Lewis, F.; Pentith, J.; Axon, A. T. R.; Dixon, M. F.; Quirke, P. Serum and gastric luminal epidermal growth factor in *Helicobacter pylori*—associated gastritis and peptic ulcer disease. *Helicobacter* **1996**, *1*, 219–226.
- (42) Weeks, D. L.; Eskandari, S.; Scott, D. R.; Sachs, G. A H⁺-Gated Urea Channel: The link between *Helicobacter pylori* urease and gastric colonization. *Science* **2000**, *287*, 482–485.

- (43) Gupta, V.; Bhavanasi, S.; Quadir, M.; Singh, K.; Ghosh, G.; Vasamreddy, K.; Ghosh, A.; Siahaan, T. J.; Banerjee, S.; Banerjee, S. K. Protein PEGylation for cancer therapy: bench to bedside. *Journal of Cell Communication and Signaling* **2019**, *13*, 319–330.
- (44) Balasubramanian, A.; Ponnuraj, K. Crystal Structure of the First Plant Urease from Jack Bean: 83 Years of Journey from Its First Crystal to Molecular Structure. *Journal of Molecular Biology* **2010**, *400*, 274–283.
- (45) Baffou, G. *Thermoplasmonics: Heating Metal Nanoparticles Using Light*; Cambridge University Press, 2017.
- (46) Wheaton, S.; Gordon, R. Molecular weight characterization of single globular proteins using optical nanotweezers. *Analyst* **2015**, *140*, 4799–4803.
- (47) Yousefi, A.; Ying, C.; Parmenter, C. D. J.; Assadipapari, M.; Sanderson, G.; Zheng, Z.; Xu, L.; Zargarbashi, S.; Hickman, G. J.; Cousins, R. B.; Mellor, C. J.; Mayer, M.; Rahmani, M. Optical monitoring of in situ iron loading into single, native Ferritin proteins. *Nano Letters* **2023**, *23*, 3251–3258.
- (48) Madan, L. K.; Welsh, C. L.; Kornev, A. P.; Taylor, S. S. The “violin model”: Looking at community networks for dynamic allostery. *The Journal of Chemical Physics* **2023**, *158*, 081001.
- (49) Feder, M. J.; Akyel, A.; Morasko, V. J.; Gerlach, R.; Phillips, A. J. Temperature-dependent inactivation and catalysis rates of plant-based ureases for engineered biomineralization. *Engineering Reports* **2021**, *3*, e12299.
- (50) Monzon, A. M.; Zea, D. J.; Fornasari, M. S.; Saldaña, T. E.; Fernandez-Alberti, S.; Tosatto, S. C. E.; Parisi, G. Conformational diversity analysis reveals three functional mechanisms in proteins. *PLOS Computational Biology* **2017**, *13*, 1–18.

- (51) Rohrbach, A. Stiffness of Optical Traps: Quantitative Agreement between Experiment and Electromagnetic Theory. *Phys. Rev. Lett.* **2005**, *95*, 168102.
- (52) Korson, L.; Drost-Hansen, W.; Millero, F. J. Viscosity of water at various temperatures. *The Journal of Physical Chemistry* **1969**, *73*, 34–39.
- (53) Grancic, P.; Illeova, V.; Polakovic, M.; Sefcik, J. Thermally induced inactivation and aggregation of urease: Experiments and population balance modelling. *Chemical Engineering Science* **2012**, *70*, 14–21.
- (54) Fishbein, W. N. Urease Catalysis III. Stoichiometry, Kinetics, and Inhibitory Properties of a Third Substrate: Dihydroxyurea. *The Journal of Biological Chemistry* **1965**, *240*, 2402–2406.
- (55) Bouloumis, T. D.; Kotsifaki, D. G.; Han, X.; Nic Chormaic, S.; Truong, V. G. Fast and efficient nanoparticle trapping using plasmonic connected nanoring apertures. *Nanotechnology* **2020**, *32*, 025507.
- (56) Kotsifaki, D. G.; Nic Chormaic, S. The role of temperature-induced effects generated by plasmonic nanostructures on particle delivery and manipulation: a review. *Nanophotonics* **2022**, *11*, 2199–2218.